M^3: Multipath Assisted Wi-Fi Localization with a Single Access Point

Zhe Chen, Guorong Zhu, Sulei Wang, Yuedong Xu*, Jie Xiong, Jin Zhao, Jun Luo, Xin Wang

Abstract—Owing to the ubiquitous penetration of Wi-Fi in our daily lives, Wi-Fi indoor localization has attracted intensive attentions in the last decade or so. Despite some significant progresses, the high accuracy of existing systems is still achieved at the cost of dense access point (AP) deployment. The more practical single AP localization is largely left as an open problem, because the hardware-induced time delay "contaminates" the measurement of signal propagation time in the air. In this paper, we design and implement M^3 to tackle this challenge with commodity Wi-Fi cards. M^3 exploits a *multipath-assisted* approach that turns the harmful multipath from foe to friend to enable single AP localization: a device can be pinpointed through the combination of azimuths and the **relative** time of flight (ToF) of Line-of-Sight (LoS) signal and reflection signals, eliminating the need for multiple APs along with their absolute ToF measurements. M^3 further utilizes frequency hopping to combine *multiple channels* to form a virtually wider-spectrum channel for higher ToF resolution. As a prominent feature of M^3, the channels do not need to be adjacent. Comprehensive experiments demonstrate that M^3 outperforms the state-of-the-art systems and achieves a median localization accuracy of 71 cm in three environments with a single AP.

Index Terms—Wi-Fi Localization, Multipath, MIMO, Multi-channel, Channel Estimation

◆

1 INTRODUCTION

LOCATION information is the key component for many applications including navigation [1], virtual/augmented reality [2], robotics [3], and security surveillance [4]. In outdoor environments, Global Position System (GPS) has achieved a big success in offering meter-level localization accuracy. However, in indoor environments, GPS signals, after penetrating through walls, become too weak to be utilized for localization due to the high attenuation. Consequently, many technologies have been explored for indoor localization, including sound [5] [7], infrared [8], visible light [9] [10], and RF [11] [12] [13] [14] [15] [16] [17] [18]. Among these technologies, Wi-Fi based solutions [11] [13] [14] [19] are particularly promising as Wi-Fi infrastructure has been ubiquitously deployed.

Wi-Fi based localization systems can be broadly grouped into three categories: fingerprint-based [20], angle-of-arrival (AoA)-based [11] and time-of-flight (ToF)-based [13]. Fingerprint-based solutions require readings from multiple APs, yet collecting the fingerprints is extremely labor-intensive. Furthermore, due to the rich mutipath indoors

and shadowing effects, the accuracy of fingerprint-base solutions is usually low. AoA-based solutions need to synthesis angle information from multiple APs for localization, but this requirement can not be fulfilled at home and small business environments that usually have only one AP. ToF-based localization is popular with ultrawide band (UWB)
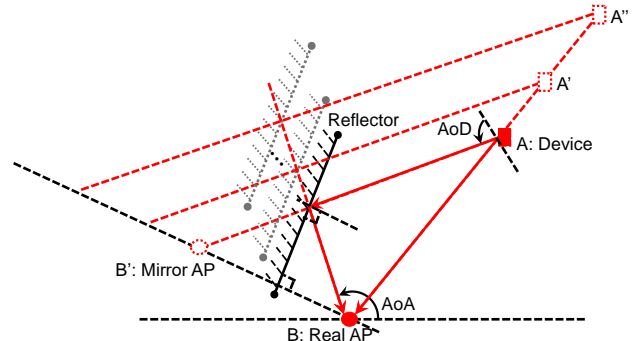

Fig. 1: An example for multipath-assisted Wi-Fi device localization

Our target in this work is to design a single AP localization system while maintaining the sub-meter accuracy in a rich multipath environment. Different from traditional approaches that consider multipath harmful, our M^3 system harnesses multipath for localization. Essentially, M^3 pinpoints the relative location of a target device with respective to a given AP. If the exact position of the AP is known beforehand, the absolute position of the target device can thus be obtained. The major obstacle is that, when there is only one AP, the AoA information alone is not sufficient to localize the device; location can be pinpointed only if both the angle (AoA) and propagation time (ToF) are available. However, without a nanosecond-level time synchronization

- *Zhe Chen, Guorong Zhu, Jin Zhao and Xin Wang are with School of Computer Science, Fudan University, Shanghai 200433, China, and also with Shanghai Key Laboratory of Intelligent Information Processing, Shanghai 200433, China. E-mail: zhechen13@gmail.com, {zhugr16, jzhao, xinw}@fudan.edu.cn.*
- *Sulei Wang and Yuedong Xu are with School of Information Science and Technology, Fudan University, Shanghai 200433, China. E-mail: {wangsl16, ydxu}@fudan.edu.cn.*
- *Jie Xiong is with College of Information and Computer Sciences, University of Massachusetts, Amherst, Massachusetts, USA. E-mail: jxiong@cs.umass.edu.*
- *Juo Luo is with the School of Computer Science and Engineering, Nanyang Technological University, Singapore 639798. E-mail: {junluo}@ntu.edu.sg.*

between the AP and device, it is impossible for us to accurately obtain the absolute signal propagation time between the two devices.

To overcome this obstacle, we exploit multipath to help localization, whose rationale is illustrated in Figure 1. With multiple antennas at both sides, we can obtain AoA information at the receiver and angle-of-departure (AoD) information at the transmitter. With AoA and AoD, we are still not able to uniquely determine the device's location as shown in Figure 1 (e.g., not able to differentiate A, A', A''), yet a single reflected path may help. Without time synchronization, though it is challenging to get the absolute propagation time, the relative time difference between the direct path and reflection path signals can be obtained. With AoA, AoD and this time difference, the reflection point can be uniquely determined and the target location can thus be estimated. Note that here we only show one reflected path. In reality, we may have multiple reflected paths and they can all be utilized to further improve the location accuracy. The opportunity here is that with the popularity of MU-MIMO [22], both the AP side and the receiver side have multiple antennas. The latest smart devices such as HUAWEI [21] have 4 antennas built in. For larger size Pads and laptops, antenna array can easily be built in. The next generation Wi-Fi protocol is considering to include 60GHz besides the current 2.4GHz and 5GHz bands and thus we expect an even smaller wavelength and larger number of antennas to be equipped in a single device in the future.

To realize this idea in practice, multiple challenges need to be tackled. First of all, commodity Wi-Fi cards usually have only 3-4 antennas. With a limited number of antennas, the AoA and AoD estimates are coarse. A even more challenging issue is that with a small 20MHz channel bandwidth, the *basic resolution* of time measurement is 50ns. This means that if the time difference is below this resolution, a naive sampling cannot obtain the time difference precisely, thus degrading the localization performance.

Inspired by [44], we jointly estimate AoA, AoD and ToF in frequency domain with a modified version of the SAGE algorithm [43]. The channel state information on each of Wi-Fi OFDM subcarrier contains the AoA, AoD and ToF of the propagation path. Mathematically, each subcarrier contributes a nonlinear equation to resolve the channel parameters. The more equations we have, the better the ToF resolution we can achieve, even though the equations originated from the same channel are correlated to a large extent. Our algorithm refines the channel estimation iteratively, outperforming the traditional subspace based approach such as MUSIC [11] and ESPRIT [24] with one-shot estimation.

To increase the time domain resolution, we combine multiple channels to form a virtually wider-spectrum channel for higher resolution. Different from the state-of-the-art system ToneTrack [13] that only combines adjacent channels, our approach is able to handle non-adjacent channels. This is particularly useful, as hopping to adjacent channels is not always feasible in reality due to crowded Wi-Fi channel usage. However, since the initial phase caused by each channel hopping may vary, we cannot perform one-time calibration. Instead, we require an extra Wi-Fi card only to calibrate initial phases several times in a AP.

To summarize, our main contributions of this paper are

as follows.

- We propose a novel approach to concatenate non-adjacent Wi-Fi channels to increase time resolution, and accordingly improve the accuracy of channel parameters (AoA, AoD, and ToF) estimation in frequency domain.
- We present a simple geometry method that uses multipath channel parameters to realize localization with only a single Wi-Fi AP.
- Our system, M^3 is implemented and evaluated with commodity Intel 5300 Wi-Fi cards. Extensive experiments demonstrate a high accuracy and significant performance improvement over the state-of-the-art systems.
- We propose the concept of mutual localization that has many real-life applications.

The rest of this paper is structured as follows. The overview of M^3 is provided in Section 2, and the detail of system design is presented in Section 3. The implementation detail and extensive experiments are discussed in Section 4 and Section 5, respectively. We summarize the related work of indoor localization in Section 6, before concluding our paper in Section 7.

2 System Overview

2.1 Important Concepts

In a typical indoor environment, the multipath signals are complicated as shown in Figure 2. All light-of-sight (LoS) and non-light-of-sight (NLoS) signals have different channel parameters. We explain each channel parameter here.
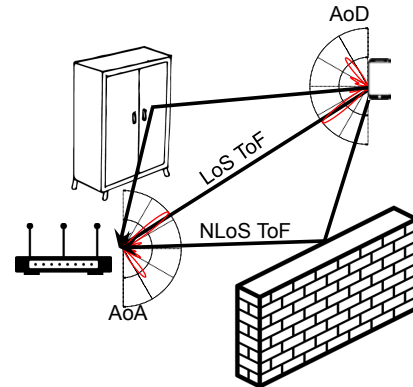

Fig. 2: Multipath signals in a typical indoor environment

Angle of Arrival (AoA). AoA means the direction of incoming signal at the receiver with an antenna array. The resolution of multipath signals is dependent on the number of antennas. With more antennas, higher angle resolution can be achieved. However, for a mobile device, the number of antennas is limited by the size of the device.

Angle of Departure (AoD). AoD is the direction of outgoing signal at the transmitter with an antenna array. Similar to AoA, the resolution of AoD is decided by the number of antennas at the transmitter.

Time of Flight (ToF). ToF is the signal propagation time from the transmitter to the receiver. ToF can be easily converted to the propagation distance by multiplying the signal speed

in the air. It is well known that the channel bandwidth is inversely proportional to the resolution of ToF. With a larger channel bandwidth, a higher ToF resolution can be achieved. *Complex Attenuation.* When wireless signal propagates from transmitter to receiver through different paths, both the amplitude and phase get changed accordingly. For each path, the complex attenuation contains both the amplitude and phase changes. The LoS signal usually experiences a smaller attenuation and thus is stronger than the multipath (reflection) signals. Moreover, the material of the reflector can also affect the complex attenuation [32]. Note that it is possible
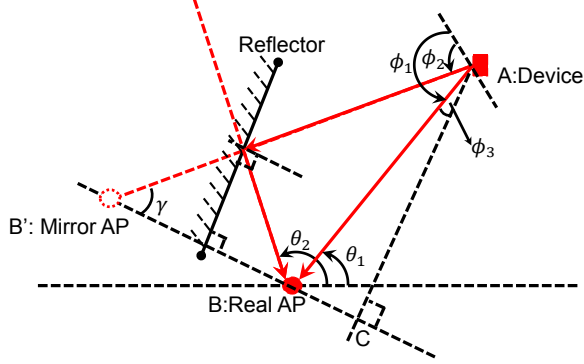

Fig. 3: Multipath-Assisted Device Localization

Different from conventional geometry methods for localization that require two or more APs, our solution leverages above geometric features of multipath, as well as LoS channel parameters to localize the target device. From Figure 3, if the AP knows AoAs (θ_1, and θ_2), AoDs (ϕ_1, and ϕ_2), relative distance calculated by relative ToF, and the speed of radio, the solid red line triangle is determined. Moreover, the reflector is also determined via reflection principle. Therefore, we can figure out a geometric approach to estimate the location of the target device. For example, the NLoS path is treated as a mirror AP to localize the target device along with the real AP. We will explain the design and implementation details of M^3 for device-based localization in the next several sections.

2.2 System Components

We hereby briefly describe the system components of M^3. We modify the SAGE algorithm to jointly estimate AoA, AoD and ToF in frequency domain, enabling a high accuracy single AP localization system. We control the channel hopping following the Wi-Fi hopping protocols [14] [17] and collect CSI readings at each channel from commodity Intel Wi-Fi card. We describe the key components of M^3 below.

- **Super-resolution channel parameter estimation:** As the prerequisite of localization, channel parameters of both LoS and NLoS paths must be extracted from the CSI readings. To achieve this goal, we modify the SAGE algorithm to jointly estimate AoA, AoD and ToF of all paths.
- **Multi-channel concatenation:** The resolution of ToF estimation is inversely proportional to the available channel bandwidth. Therefore, we propose a novel

channel concatenation scheme to stitch channels, so as to improve the ToF resolution. With the proposed method, even non-adjacent channels can be stitched together to form a virtually larger channel bandwidth for a higher time resolution.

- **Multipath-assisted device localization:** With the channel parameters of the LoS and reflection paths, we derive a mathematical model to obtain the location estimation for the target device with respect to the AP. For multiple candidate positions calculated from multiple reflection paths, we propose an optimization algorithm to determine the final location estimation.

3 SYSTEM DESIGN

In this section, we design a unified approach to jointly estimate AoA, AoD and relative ToF that are the core-stones of the single-AP enabled indoor localization.

3.1 Wireless Channel Model

To begin with, we describe the wireless channel model that captures the propagation of waves in the air. Considering a transmitter (device) with M antennas and a receiver (AP) with N antennas. Each channel is partitioned into a set of K subcarriers where the carrier frequency is f and the kth subcarrier frequency is f_k for all $1 \leq k \leq K$. The rich reflections in indoor environments yield P major propagation paths between the transmitter and the receiver. The wireless channel on path p is represented by a four-parameter tuple $\eta_p = \{\alpha_p, \theta_p, \phi_p, \tau_p\}$, where α_p denotes the complex amplitude, θ_p denotes the AoA to the receiver, ϕ_p denotes the AoD from the transmitter and τ_p is the ToF. Let $s(f)$ be the transmitted signal to the AP at the frequency domain, and let $\mathbf{y}(f_k, \eta_p)$ be the vector of received signal at the kth subcarrier on the pth path. Denoting λ as the wave length and d as the spacing between two adjacent antennas. d is set as $\lambda/2$ to avoid spatial aliasing. We thus obtain:

$$
\begin{aligned}
\mathbf{y}(f_k; \eta_p) &= \mathbf{H}(f_k; \eta_p) + \mathbf{N}(f) \\
&= \alpha_p \mathbf{c}(\theta_p) \mathbf{g}^T(\phi_p) e^{-j2\pi\tau_p f_k} s(f) + \mathbf{N}(f), \quad (1)
\end{aligned}
$$

where

$$
\begin{aligned}
\mathbf{c}(\theta_p) &:= [1, e^{-j2\pi d \cos(\theta_p)/\lambda}, \cdots, e^{-j2\pi d(N-1)\cos(\theta_p)/\lambda}]^T; \\
\mathbf{g}(\phi_p) &:= [1, e^{-j2\pi d \cos(\phi_p)/\lambda}, \cdots, e^{-j2\pi d(M-1)\cos(\phi_p)/\lambda}]^T.
\end{aligned}
$$

We also denote $\mathbf{H}(f_k; \eta_p) = \alpha_p \mathbf{c}(\theta_p) \mathbf{g}^T(\phi_p) e^{-j2\pi\tau_p f_k}$. In practice, the received signal on subcarrier k is the aggregation of signals from all the paths, i.e., $\mathbf{y}(f_k) := \sum_{p=1}^{P} \mathbf{y}(f_k; \eta_p)$.

Our single-AP localization enforces a rather simple logic: the AP estimates the direction of the device and the wave propagation delay from the device to the AP.

3.2 Super-Resolution Channel Parameters

The subspace-based approach such as MUSIC [11] extracts the path parameter of multipath in one shot by decomposing the covariance matrix of the signal into a signal subspace and a noise subspace. SAGE algorithm [44] further pursues the optimal estimation of channel parameters in an iterative
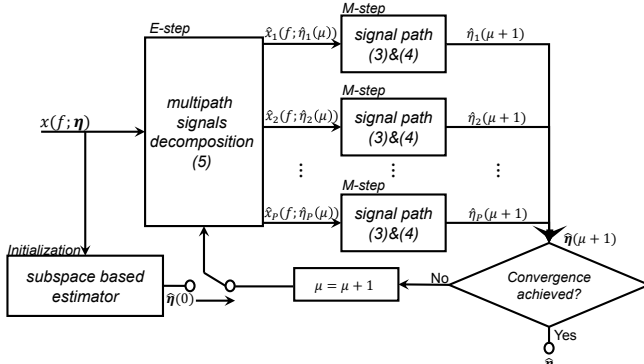
Fig. 4: The signal flow graph of M^3 at $(\mu+1)^{th}$ iteration. The symbol $x(f, \boldsymbol{\eta})$ represents the input variables.

approach. Our design is also inspired by [44] designed in time domain, but we extend their SAGE algorithm to SAGE+ in frequency domain for our purpose.

The flow chart of parameter estimation is shown in Figure 4. To avoid local minimum issue of SAGE+ algorithm, we utilize a one shot estimation approach based on the subspace method (in Section 3.2.2) to find proper starting points. After initialization, the coarse channel parameters of each path are injected to SAGE+ algorithm for a finer estimation (detailed in Section 3.2.1).

3.2.1 Maximum Likelihood Estimation

According to [43], [44], we can obtain the following likelihood function in frequency domain:

$$z(\tau_p, \theta_p, \phi_p) = \sum_{k=1}^{K} \mathbf{c}^H(\theta_p) x_p(f_k; \eta_p) \mathbf{g}^\star(\phi_p) e^{j2\pi\tau_p f_k}, \quad (2)$$

where the symbol $\star$ means conjugation operation, and x_p represents the pth signal, such as CSI. Therefore, the SAGE+ algorithm can iteratively estimate η_p by maximizing the following equation:

$$(\hat{\phi}_p, \hat{\theta}_p, \hat{\tau}_p)_{est} = arg \max_{\phi_p, \theta_p, \tau_p} |z(\phi_p, \theta_p, \tau_p)|. \quad (3)$$

From Eq. (1) and (3), the amplitude α_p can be derived

$$\hat{\alpha}_p = \frac{1}{K \cdot N \cdot M} z(\phi_p, \theta_p, \tau_p). \quad (4)$$

With the above steps, we can adopt P paths channel parameters $\hat{\eta} = \{\hat{\eta}_1, \hat{\eta}_2, \cdots, \hat{\eta}_P\}$ to reconstruct an "expected" single path signal. The single path is expressed as

$$\hat{x}_p(f_k; \hat{\eta}_p) = x_p'(f_k; \hat{\eta}_p) + \beta_p \left[x(f_k; \eta) - \sum_{p=1}^{P} x_p'(f_k; \hat{\eta}_p) \right] \quad (5)$$

where $x(f_k; \eta) = \sum_{p=1}^{P} \mathbf{H}_p(f_k; \eta_p)$ represents the original input signals.

For further reducing the complexity, we employ a coordinate-update approach instead of exhaustive search [43], [44]. The coordinate-update approach for each path signal executes as following:

$$(\theta_p'')_{est} = arg \max_{\theta_p} |z(\tau_p', \theta_p, \phi_p')|, \quad (6)$$

$$(\phi_p'')_{est} = arg \max_{\phi_p} |z(\tau_p', \theta_p'', \phi_p)|, \quad (7)$$

$$(\tau_p'')_{est} = arg \max_{\tau_p} |z(\tau_p, \theta_p'', \phi_p'')|. \quad (8)$$

In other words, we only search one parameter in each iteration, while fixing the other two parameters. In this way, the search space dimension is reduced from $T_\theta \times T_\tau \times T_\phi$ to $T_\theta + T_\tau + T_\phi$. The above SAGE algorithm still performs the expectation step Eq. (5), and the maximization step Eq. (3) and (4). Therefore, this iterative process is essentially an Expectation Maximization (EM) algorithm, and the convergence can be guaranteed [57]. The cost of this approach is that we cannot guarantee the global maximum. For example, if there are two similar signals merged together, and there is no a priori knowledge, the algorithm probably falls in local minimums. However, with a good starting point, the risk of missing the global maximum is very low.

3.2.2 Subspace Estimation

The above algorithm relies on a good starting point to initiate; otherwise it may either have a slow convergence rate or be trapped into local minimums [57]. Therefore, we utilize a 3D subspace-based approach to provide a rough estimation of channel parameters first. These initial estimations are then used to initialize the SAGE+ algorithm that refines the estimation step by step.

The subspace approach requires the construction of the auto-correlation matrix of signals. To achieve this goal, we vectorize $\mathbf{H}(\eta)$ from a $M \times N \times K$ dimensional channel matrix into a vector with $\Gamma = M \cdot N \cdot K$ complex elements: $\mathbf{u}(\eta) = vec(\mathbf{H}(\eta))$. The auto-correlation matrix of the CSIs is calculated as $\mathbf{R_u} = \mathbf{u}^H \mathbf{u}$. According to [12], the noise subspace and the signal subspace are orthogonal in the auto-correlation matrix. Hence, we adopt the singular value decomposition method to extract the signal subspace for the estimation of multi-path channel parameters. Given P paths between the AP and the device, the noise subspace matrix denoted by $\mathbf{E}_n$ has the dimension of $\Gamma \cdot (\Gamma - P)$. Denoting by $\mathbf{e}(\tau)$, the $K \times 1$ vector in which the kth element is $e^{j2\pi f_k \tau}$, we then formulate an optimization problem to estimate $\{\eta_1, \cdots, \eta_P\}$ as the following:

$$\{\eta_1, \cdots, \eta_P\}_{est} = arg \min_{\phi, \theta, \tau} \left| \left(\mathbf{g}(\phi) \bigotimes \mathbf{c}(\theta) \bigotimes \mathbf{e}(\tau) \right)^H \mathbf{E}_n \right|^2, \quad (9)$$

where the symbol $\bigotimes$ represents the Kronecker product operator. Similar to [12], [15], we also perform smoothing operation via subsets of transmit antennas, receive antennas, and sub-carriers. Note that the above optimization problem cannot be used to estimate the complex attenuation α in each path. After each $(\eta_p)_{est}$ being estimated, we calculate the complex attenuation $(\alpha_p)_{est}$ with Eq. (4), and reconstruct the signal according to Eq. (1). Finally, the vectors of multi-path parameters $\{\eta_1, \cdots, \eta_P\}$ are chosen as the starting point of the EM iteration procedure. We only use the subspace estimation results once for initialization in a base channel but not all hopping channels. Furthermore, there are approaches with reduced complexity to accelerate the subspace estimation, such as [65], [66], making subspace estimation for initialization feasible.

3.3 Multi-Channel Concatenation

The indoor localization is a nice example of "Bucket Theory", that is, its precision is determined by the channel

parameter with the worst resolution. The relative ToF is the most difficult parameter to be accurately estimated because even an error of merely 1ns corresponds to a propagation distance of 0.3 meter. The resolution of ToF estimation relies on a large spectrum width, usually much larger than a single 20MHz Wi-Fi channel. This motivates our design to concatenate multiple channels for improving ToF resolution.

3.3.1 Multi-Channel Concatenation vis Channel Hopping

Channel hopping provides a possibility to augment spectrum width for improving ToF estimation, while complying with 802.11 specifications. For instance, [13] and [33] utilize channel hopping to collect CSIs from a set of adjacent channels and merge them to refine ToF resolution. However, augmenting spectrum via channel hopping often has a stringent requirement that all the hoppings need to be completed within the coherence time (e.g., ∼ 10ms indoors). If hopping has to take a predefined sequences (e.g., adjacent channels), it is much more likely to hop into a channel occupied by ongoing transmissions, causing CSIs measurement duration to exceed the coherence time. In view of this limitation, it is crucial to devise a more flexible scheme able to make use of arbitrary channels.

According to [32], only the complex attenuation of the received signal changes after the coherence time when the device is not moving and the environment remains the same. This property allows us to synthesize the CSIs of arbitrary channels under the EM framework regardless of the violation of coherence time.

3.3.2 Multi-Channel Concatenation Approach

We reformulate the objective function Eq. (2) of our multi-dimensional estimation problem so as to incorporate the CSIs of multiple channels. Denoting by I the set of available channels used for localization. The new likelihood function is given by

$$z(\tau_p, \theta_p, \phi_p) = \sum_{i \in I} \sum_{k=1}^{K} \mathbf{c}^H(\theta_p) \mathbf{H}(f_{i,k}; \eta_p) \mathbf{g}^\star(\phi_p) e^{j2\pi\tau_p f_{i,k}},$$
(10)

where $f_{i,k}$, with certain abuse of notation, is the frequency of the kth subcarrier on channel i. The benefit brought by this modification is that we acquire more samples of channel impulse response but with the same number of unknown parameters. The more channels being used, the more equations will be involved in Eq. (10) and hence the more accurate estimation of ToF can be achieved.

We conduct a set of controlled experiments to verify the feasibility of non-continuous channel concatenation. Two RF cables are used to emulate two propagation paths in a wireless channel. We adjust the difference of their lengths to mimic different multi-path environments. Given the wave propagation rate of 2×10^8 m/s in copper cables, the relative ToFs are 13.5ns, 23.5ns, and 38.5ns when the path length differences are 2.7m, 4.7m and, 7.7m respectively. Up to ten channels at 5GHz band are concatenated. Figure 5. illustrates the outcomes of our multi-dimensional estimation with the different number of channels, where x-coordinate represents the value of ToF and y-coordinate represents its likelihood. Basically, a peak indicates the emergence of an
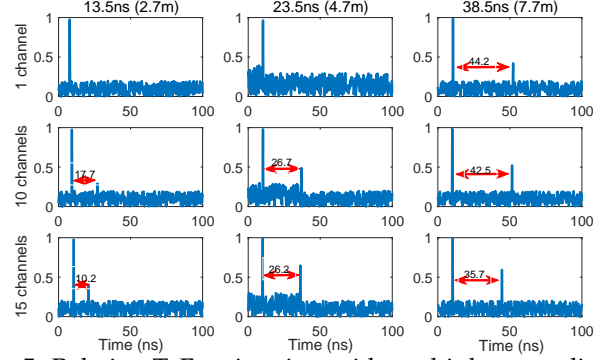

Fig. 5: Relative ToF estimation with multiple non-adjacent channels.

identifiable propagation path. When the distance difference is 2.7m, only one dominant ToF is observed in the single channel case, hence the two paths cannot be separated. With 10 channels concatenated, the second peak appears with a relative ToF of 17.75ns, though still bearing a big gap to the ground truth. Further concatenating the 15 channels, the relative ToF between two paths exhibit a lower error of 3.25ns. When the distance difference is 7.7m, the two paths can be separated even with a single channel, but the relative ToF becomes more accurate with the measured CSIs in 15 channels. Therefore, concatenating multiple non-continuous channels will improve the ToF resolution especially in the situations where the multi-path distances are relatively close to each other.

3.4 Multipath-Assisted Device Localization

Recall that the exact ToF cannot be accurately estimated because of the extra delay introduced at the circuit modules of the transmitter and the receiver. This physical constraint causes an over-estimation of the propagation distance. We hereby explore the geometric pattern of multi-path reflections to localize the device using the relative ToFs instead of the exact ones.

We employ a simple example to illustrate the principle of multi-path assisted device localization in Figure 3. The A and B denote the locations of the device and the AP, respectively, and these exist a direct LoS path and a reflection path between A and B. Moreover, B′ is the mirror of B with respect to the reflector. The location of the AP is assumed to be the origin, and the location of the device is denoted by (x_A, y_A). The AoA and the AoD of the direct path are θ_1 and ϕ_1, and those of the reflection path are θ_2 and ϕ_2. Let $d_{AB'}$ (resp. $d_{AB'}$ and $d_{BB'}$) be the distance of the line segment "AB" (resp. "AB′" and "BB′"). The relative ToF between the direct path and the reflection path is $(\tau_2 - \tau_1)$, equivalent to the wave propagation time for a distance of $(d_{AB'} - d_{AB})$. Therefore, the indoor localization reduces to a simple geometry problem: *Given θ_1, θ_2, ϕ_1, ϕ_2 and $(d_{AB'} - d_{AB})$, how can the distance d_{AB} be derived?*

After certain manipulations, the angle γ is expressed as

$$\gamma = \frac{\pi - (\phi_1 - \phi_2) - (\theta_2 - \theta_1)}{2}.$$

We then draw a perpendicular line from A toward the line "B'B" with the foot C, which further gives:

$$\phi_3 = \frac{\pi}{2} - \gamma - (\phi_1 - \phi_2);$$
$$d_{AB'} \sin(\gamma) = d_{AB} \cos(\phi_3);$$
$$d_{AB'} - d_{AB} = (\tau_2 - \tau_1) \cdot c.$$

Combining the above equations together, we obtain the distance d_{AB} as follows:

$$
\begin{aligned}
d_{AB} &= \frac{c(\tau_2 - \tau_1)\sin(\gamma)}{\cos(\phi_3) - \sin(\gamma)} \\
&= \frac{c(\tau_2 - \tau_1)\cos(\frac{(\theta_2-\theta_1)+(\phi_1-\phi_2)}{2})}{2\cos(\frac{(\theta_2-\theta_1)}{2})\cos(\frac{(\phi_1-\phi_2)}{2})}
\end{aligned}
\tag{11}
$$

From Eq. (11), d_{AB} depends only on AoAs (θ_1, θ_2), AoDs (ϕ_1, ϕ_2), and relative ToF $(\tau_2 - \tau_1)$. Consequently, the need for absolute ToF measurement is totally removed, and the coordinate of the device is computed as $(d_{AB}\cos(\theta_1), d_{AB}\sin(\theta_1))$. In this way, our system pinpoints the relative position of the target device. If the position of AP is known in advance, the absolute location of the target device can be obtained.

Relying on only one reflection path is prone to be corrupted when the parameter estimation of this path happens to be poor. Incorporating more reflection paths will improve the robustness of the localization. With P paths (a direct path and $P - 1$ reflection paths), one may obtain $P - 1$ locations of the AP. Denote by (A_x^p, A_y^p) the coordinate of the device determined by the pth reflection path and the direct path. The optimal localization problem is to search the coordinate (A_x^*, A_y^*) that minimizes the aggregate Euclidean distance from the $P - 1$ estimated locations to it.
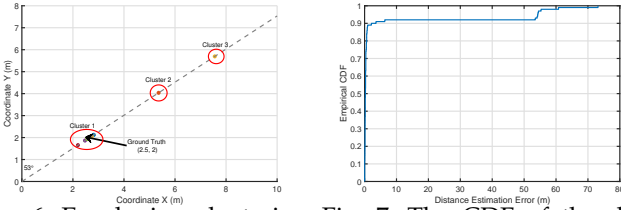
3.5 Filtering Higher Order Reflection

Fig. 6: Employing clustering to remove higher order reflections

Fig. 7: The CDF of the distances d_{AB}s' estimation errors

Our system utilizes only first order reflections for localization while treating the higher order reflections as interference, because the signal strength of higher order reflections is usually weak. In some situations, the higher order reflections can be identified, but their relative ToFs can often be much larger than those of the first-order reflections, since the reflected signals traverse a much longer distance. Therefore, the higher order reflections either barely influence the accuracy or can be readily ruled out.

The most distinctive characteristic of high-order reflection paths, due to their large relative ToFs, is that the localization assisted by them often leads to larger errors. We conduct experiments to validate our claim. We extract the path parameters of direct path and several reflection paths in a multipath-rich environment, and use them to estimate positions accordingly. We show the localization results for each reflection path and LoS in Figure 6. Since the AoA of LoS is unique, all the localization results lie in a single line in experiments. The localization results closest to the ground truth forms cluster 1, while the far larger relative ToF values (potentially indicating high-order reflections) lead to other clusters far away from cluster 1. Such a discrepancy might stem from the fact that the first order reflection geometry model does not fit the higher order reflections [64]. We also plot the CDF of distances d_{AB}s' estimation errors in Figure 7. Obviously, only about 7% estimated distances are much larger, showing that the majority of reflections are still the first order reflection.

In reality, we indeed apply a clustering method to exclude the higher order reflections from participating in estimating the device location. Basically, after estimating the location of target device based on all NLoS and LoS signals via the method discussed in Section 3.4, we employ Density-Based Spatial Clustering of Applications with Noise (DBSCAN) [36], a non-parametric algorithm, to cluster all location points. Provided with a set of estimated locations in a space, DBSCAN algorithm can group points closest to each other, and exclude outlier points that are in low-density regions. In most of indoor environments, there often exist a number of dominant reflectors, and first order reflections are usually much stronger than higher order reflections thanks to channel attenuation. Therefore, we still can utilize the majority of location estimations to synthesize the final estimation. We leave some further discussions to Appendix C.

4 IMPLEMENTATION

We implement M^3 on the off-the-shelf Intel 5300 Wi-Fi card. The CSI TOOL [58] is used to measure channel state information on 5GHz Wi-Fi bands. Although Wi-Fi card transmits over 128 OFDM subcarriers at 40MHz, the CSI TOOL only provides 8-bit quantized real and imaginary values on 30 subcarriers. Therefore, we interpolate the missing CSI on the remaining subcarriers.

Our system consists of several laptops equipped with Intel 5300 cards. The laptop is configured with 4GB Random Access Memory (RAM), 500 GB hard disk and Intel Core i7-4500U 1.80GHz CPU. All these laptops operate at the monitor mode. Each antenna is placed with a spacing of 2.7 cm (nearly $\frac{1}{2}$ wavelength of 5GHz band), which is shown in Figure 8. With such a small antenna spacing, the antenna array can be readily integrated in up-to-date mobile devices. A practical challenge of M^3 indoor localization is that the raw phases of signals cannot be applied directly to estimate AoA, AoD and ToF, as they are impaired by distortions of RF oscillator offset, Sampling Timing Offset (STO) and Packet Detection Delay (PDD). In what follows, we show how the raw phases are cleaned to obtain the "true" phases of the reflecting multipath signal propagations.

Calibration for AoA and AoD. RF oscillator phase offset always exists. Each RF chain is locked by phase-locked loops (PLL) at different phase offsets. In general, these phase offsets do not change until the reset of Wi-Fi oscillator. The existence of phase offsets causes the miscalculation of phase changes of signal propagation in the air. Therefore, the phase
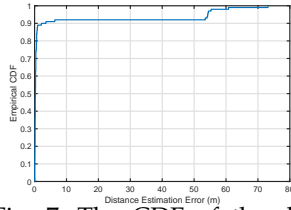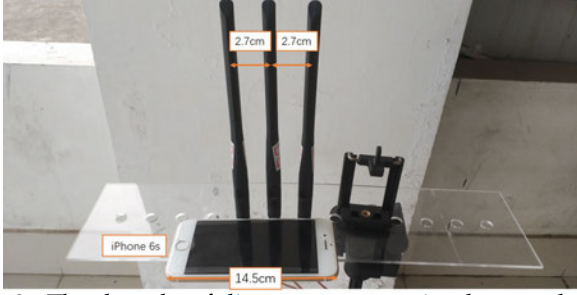
Fig. 8: The length of linear antennas is shorter than a smartphone

calibration is a preliminary step of state-of-the-art indoor localization systems [11], [12], [15], [17], [29]. In this paper, we propose a separated calibration scheme, but we leave the details to Appendix A.

Sanitizing ToF. ToF estimation on commodity Wi-Fi is also contaminated by random phase shift due to sampling time offset (STO) and packet detection delay (PDD). The STO and PDD have the same impacts on all links, because the radios on the same transceivers are time-synchronized. Therefore, a ToF sanitization algorithm similar to that in [15] is applied to remove the phase offset introduced by hardware.

5 EVALUATION

5.1 Experiments Setup

5.1.1 Deployment

We deploy our system in a variety of indoor environments including rooms of different sizes and different amounts of multipath. Figure 9 shows the layouts of four scenarios: the first is a small-size conference room ($3.2 \times 2.8 \mathrm{m}^2$) with strong multipath reflections; the second is a median-size meeting room ($6.5 \times 4.8 \mathrm{m}^2$) with moderate multipath reflections; the third is a large-size classroom ($13.5 \times 6.3 \mathrm{m}^2$) with few multipath reflections; the fourth is the corridor ($10.5 \times 2.2 \mathrm{m}^2$) with irregular walls and corners. The snapshots of these experimental environments are also shown in Figure 9. The target locations are marked as blue circles and the AP locations are marked as a small red rectangle. Our system hops over fifteen channels in 5GHz frequency, and the set of channels are indexed as {36, 44, 48, 52, 60, 64, 100, 108, 116, 120, 124, 132, 136, 149, 157}. In each channel, the packet transmission rate is set to 200pkts/s. Moreover, the height of the device is fixed in all experiments except for studying the impact of heights in Section 5.3.8.

5.1.2 Compared Approaches.

We compare M^3 with the state-of-the-art Wi-Fi CSI-based localization systems. For the micro-benchmark evaluation, we implement a modified version[1] of SpotFi [15] to estimate AoD and ToF together. We further extend SpotFi from two-dimensional MUSIC (MUSIC-2D) to three-dimensional MUSIC (MUSIC-3D) [63] to jointly estimate AoA, AoD, and ToF. We use laser meter along with building layout to measure all ground truth locations and orientations. For ToF benchmark

1. The original SpotFi estimates AoA and ToF simultaneously. We modify it to estimate AoD and ToF.

comparisons, we implement Chronos [14], the best-known ToF-based localization system. Chronos employs a different method to combine non-adjacent Wi-Fi channels to obtain more accurate ToF estimates. We do not compare the localization accuracy directly with Chronos because it requires a 30 cm spacing of pairwise antennas, thus not working with a 2.7 cm spacing in our system.

5.2 Micro-benchmark

Before presenting the localization accuracy, we conduct micro-benchmark experiments to show how well our system can perform in estimating each channel parameter. These results will help us to understand and appreciate the effect of each component of our system.

5.2.1 Accuracy of AoA estimation

We first compare the accuracy of direct path AoA of our system with SpotFi and MUSIC 3D. Figure 10 shows that our system outperforms MUSIC 3D and SpotFi. M^3 achieves a median AoA accuracy of 5.2 degrees, while those of MUSIC 3D and SpotFi are 8.6 and 9.6, respectively, in the same settings. Both M^3 and MUSIC 3D achieve a better accuracy than SpotFi because these two approaches jointly estimate three-dimensional channel parameters (AoA, AoD, and ToF) while SpotFi only estimates two-dimensional parameters (AoA and ToF). M^3 outperforms MUSIC 3D for that the former employs the maximum likelihood approach and the extended SAGE algorithm to refine channel estimation iteratively, while the latter adopts the subspace based approach for a one shot estimation that may experience serious performance degradation with low SNR [11]. It is worth noting that, as all the experiments are conducted on the *same* and the *single* channel for fair comparison, the performance gain of M^3 mainly comes from maximum likelihood approach that is nearly optimal.

5.2.2 Accuracy of AoD estimation

We also evaluate the accuracy of direct path AoD estimation in Figure 11. M^3 achieves a median AoD accuracy of 7.9 degrees compared to 12.8 degrees of MUSIC 3D and 13.2 degrees of SpotFi. This improvement is due to the same reason, that is, the three-dimensional joint channel estimation with iterative refinement. However, no matter which approach is applied, accuracy of AoA estimation outperforms that of AoD estimation. One reason lies in the different ways of acquiring signals for AoA and AoD estimation. In Wi-Fi communication, AoA is estimated using the phases of received signal at the same slot, while AoD is estimated using the phases of consecutive time slots. Therefore, any subtle misalignment undermines the accuracy of AoD estimation. The other reason is that we estimate AoA before AoD, so the error propagates from AoA to AoD, and hence get amplified.

5.2.3 Accuracy of reflected AoA and AoD estimation

Measuring the ground truth of AoA and AoD is easy for the directed path, while it is extremely difficult for the reflecting paths on the contrary. To assess the performance of path separation, we conduct a set of controlled experiments with two single reflecting paths. Two commodity Wi-Fi cards
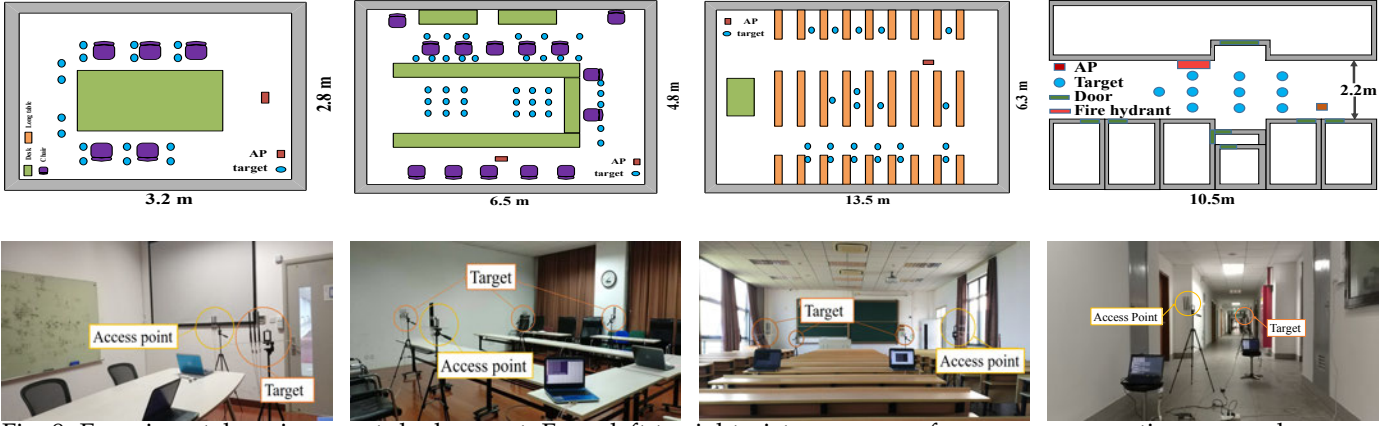
Fig. 9: Experimental environment deployment. From left to right pictures are conference room, meeting room, classroom and corridor, respectively.
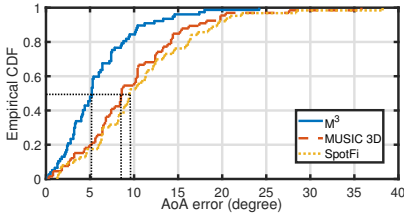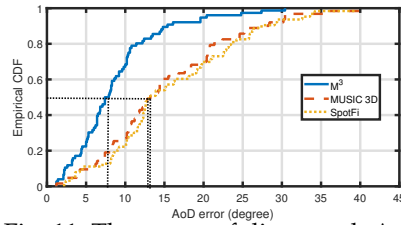

Fig. 10: The errors of direct path AoA

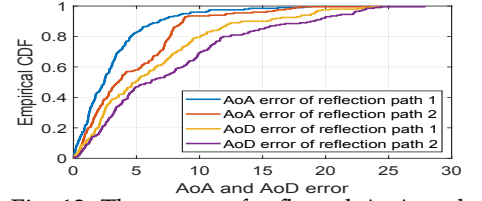Fig. 11: The errors of direct path AoD

Fig. 12: The errors of reflected AoA and AoD.

are used as the transmitter and the receiver, connected by different coaxial cables using three *different* RF chains. We vary the lengths of three cables to emulate different propagation time in the air. To emulate one AoA LoS path and two AoA reflected paths, we use nine coaxial cables in total since there are three RF chains in a commodity Wi-Fi card. For emulating three AoDs, the number of coaxial cables is same as AoAs. Figure 12 demonstrates the CDF of AoA and AoD errors of the reflecting path. We observe that the median errors of two reflected AoAs are around 2.5 and 3.4 degrees, respectively, and the median errors of two reflected AoDs are 4.9 and 6.2 degrees. Therefore, it is reasonable to conclude that our system achieves a highly accurate estimation of the channel parameters of reflecting path(s).

5.2.4 Accuracy of Relative ToF estimation
We select the most outstanding Chronos system for comparison. Because it is extremely difficult to create a reflection path that the signal propagates along a predetermined angle and is reflected at a predetermined point, we let the signal go through cables of different lengths to mimic the direct and the reflecting paths. The differences between two cables are chosen to be 2.7m, 4.7m and 7.7m, respectively. Chronos utilizes 20 Wi-Fi channels, while M^3 tries 10, 15 and 20 channels, respectively. Figure 13 shows that even with 10 channels, M^3 achieves a better accuracy of the relative ToF than Chronos. The reasons for such an improvement are two-fold. On one hand, Chronos adopts Inverse Non-uniform Discrete Fourier Transform (INDFT) approach to compute the relative ToF. It requires that the channels are separated sufficiently in the Wi-Fi unlicensed spectrum, i.e., some of them in 2.4GHz and some others in 5GHz band. When all the channels are sampled from either 2.4GHz

or 5GHz, the accuracy of Chronos degrades considerably and that of M^3 is unaffected. On the other hand, INDFT, being a sparse compressive approach, can be inferior to the maximum likelihood approach in principle [43].

5.3 Accuracy of Localization
In this subsection, we evaluate the end-to-end localization accuracy of our system in different scenarios.

5.3.1 Overall Performance
We compare the accuracy of localization with state-of-the-art algorithms in different indoor environments (conference room, meeting room, and classroom) in Figure 14. In our experiments, we fix the same height for both device and AP. The target system for comparison is MUSIC 3D [63], a premier algorithm that uses a subspace approach to jointly estimate AoA, AoD and relative ToF. We have carefully chosen the sysem to compare with, as M^3 and MUSIC 3D can fairly operate in the same scenario. We do not compare M^3 with SpotFi because SpotFi requires multiple APs. We do not compare M^3 with Chronos either because Chronos demands a wide range of channels ranging from 2.4GHz to 5GHz, and hence performs poorly with channels selected only from 5GHz. Figure 14 shows that more hopping channels yield a better accuracy of localization for M^3. When 1, 5 and 15 channels are employed, the median localization errors are 100 cm, 81 cm and 71 cm, respectively. This demonstrates that our channel combination scheme has indeed taken effect. We can also see that M^3 is still better than MUSIC 3D with a single channel. This is because the proposed EM-based super-resolution algorithm is more efficient: even when the received signals are close to each other, there is still a high chance to separate them.
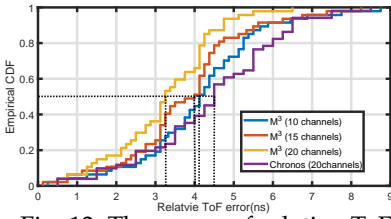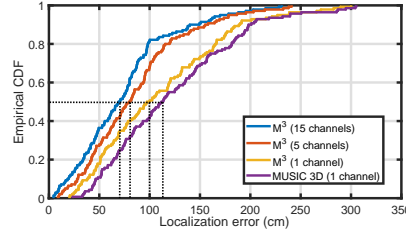
Fig. 13: The errors of relative ToF
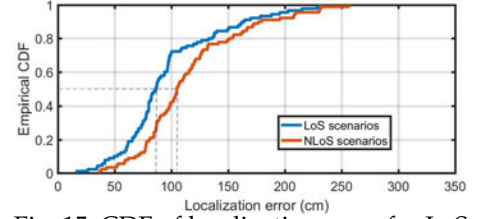

Fig. 14: Overall performance

Fig. 15: CDF of localization error for LoS and NLoS (with 15 channels)

5.3.2 Evaluation in LoS and NLoS scenarios

To demonstrate this part, we measure the localization error in the NLoS scenario. NLoS means the direct path is not always stronger than other paths, and it is not blocked totally. To create the NLoS condition, we use a wood brick (height: 50 cm; width:30 cm; thickness: 10 cm) to block the LoS signal, and conduct the localization experiments in the meeting room. From Figure 15, we can find that the median error of NLoS scenario (105 cm) is indeed larger than LoS. The reason is when we block the LoS signal, the direct path becomes weak, and is hard to be distinguished accurately from strong multipath signals. Therefore, it can introduce more errors in AoA, AoD and ToF estimations, and hence degrade overall localization performance.

5.3.3 Impact of Environments

Here, we illustrate the impact of different environments in Figure 16. In this experiment, we employ fifteen 40MHz Wi-Fi channels in the 5GHz band. In the conference room, M^3 achieves the best performance with a median localization error of 33 cm. The reasons are two-fold. One is that in a small room, the SNR is large and multipaths are rich. Both high SNR and rich multipaths help to improve accuracy. The other reason is that the localization error has an almost linear relationship with distance when AoA and AoD are employed. So a smaller room with short distances can thus achieve higher localization accuracy. We further observe that the localization errors in the meeting room and classroom are close to each other. The median localization error in the corridor is 95 cm, larger than those in the conference room, meeting room, and classroom. The reason lies in that the multipaths of wireless signals are more complicated in the corridor because of the doors, windows, and irregular walls (as shown in Figure 9). For instance, a device close to walls and corners may lead to larger errors in the channel parameter estimation phase of our system.

5.3.4 Impact of Moving Objects

We hereby evaluate the impact of moving objects on the accuracy of localization. Two volunteers are asked to walk randomly with normal speeds in the meeting room that generates irregular interfering reflection paths. Figure 17 plots the CDF of localization accuracy with walking persons. The median error increases by 28 cm compared with that without moving objects. The main reason for the degraded accuracy is that the estimates of AoA, AoD and relative ToF are impaired by the uncertain and time-varying reflection paths. However, such a gentle degradation reflects the robustness of M^3 in an adversary environment.

5.3.5 Impact of Moving Device

To understand how M^3 is influenced by the mobility of device, we evaluate the accuracy of localization when the volunteer holding the device walks for about 4 meters at a normal speed (e.g., 0.8m/s to 1m/s). For the purpose of proving the concept, only a single channel is used in this experiment. The benchmark experiments without device mobility are conducted by assuming that the device is randomly placed on the trajectory of movement. Figure 18 shows the cdf of localization accuracy where the median error increases from 120 cm to 138 cm on a single channel. When more channels are concatenated by the moving device, the accuracy of localization is better than that without channel concatenation. Nevertheless, static device has better improvement via channel concatenation than moving device. Therefore, in order to achieve higher accuracy of localization, the user should move slowly. The movement of the volunteer causes the change of multipath propagations, thus reducing the accuracy of estimating AoA, AoD, relative ToF, and in turn the accuracy of final localization. Our experiments show that M^3 is only moderately affected by device movement at a normal speed.

5.3.6 Impact of Number of Packets

We evaluate the performance of localization with different number of packets. Figure 19 shows that with increasing number of packets from 1 to 30, the median localization error are decreased slightly from 71 cm to 63 cm. It indicates that more packets can improve the localization performance, because a higher time diversity may help to reduce errors. In reality, using more packets do not introduce a large overhead in 802.11ac with 80MHz bandwidth, so we recommend to use at least 20 packets for each location estimation.

5.3.7 Impact of Distances

The impact of distances between AP and target device on the localization error is evaluated. We let the target device move along a corridor to vary the distance from 100 cm to 800 cm at a step size of 100 cm. We repeat the experiments 50 times at each location and average the results. The localization errors are shown in Figure 20. It is clear to see that the error grows with an increasing distance. We attribute this error growth to the lower receiving SNR caused by longer distances.

5.3.8 Impact of Heights

In this set of experiments, we evaluate the accuracy of localization by changing the height of the device. Our purpose is to mimic a wide range of realistic situations including
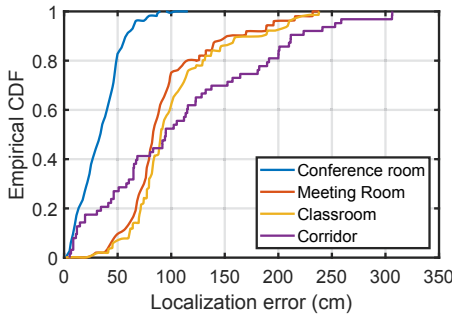
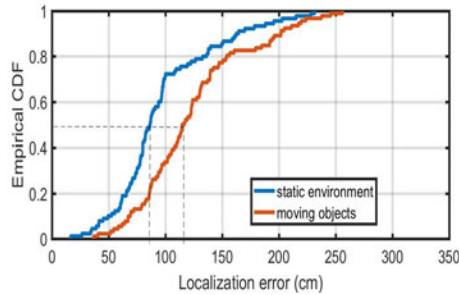Fig. 16: Impact of Deployments (with 15 channels)

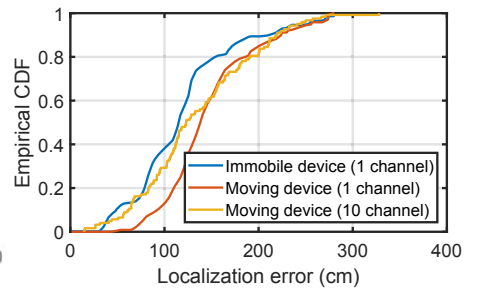Fig. 17: Impact of Moving Objects (with 15 channels)

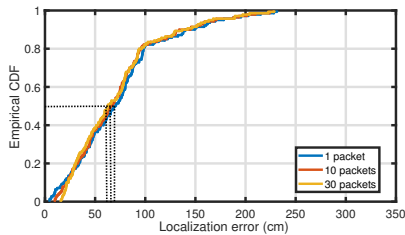Fig. 18: The CDF of localization error for moving device

Fig. 19: The CDF of localization errors with 15 channels
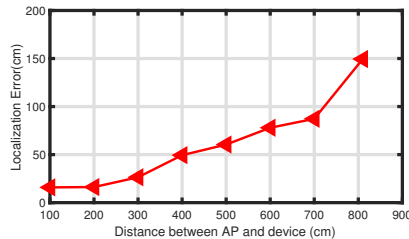

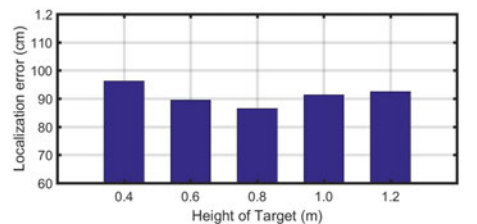Fig. 20: Impact of distances between AP and target device (with 15 channels)

Fig. 21: Impact of heights between AP and target device (with 15 channels)

that the device is hold by users of different heights, and the device is placed on a table or a chair. The height of the AP is fixed to be 0.8m above the ground since it is usually placed on a table or a cabinet at home. The height of the device in our experiments changes from 0.4m to 1.2m with a step size of 0.2m. Figure 21 shows the average localization error for each height. When the height of the device is 0.8m, i.e., on the same plane as the AP, the average error is the smallest. The localization error increases as the device deviates from the horizontal plane of the AP's antenna array. At the height of 0.4m, the device can be positioned with a mean error of 96 cm, only 10 cm larger than that at the height of 0.8 cm. Therefore, M^3 is robust even when the AP and the device are not exactly at the same height.

5.3.9 Channel Parameters Changes with Time

We change the total multipaths from 2 to 10 in a room. However, we cannot ensure all paths can be estimated, even we have set the number of multipaths. The reason is that the energy of residue signals can be too low to extract a path. We also find that in many cases, five paths can be estimated in a room. Hence, we place the target device in a fixed location, and let it transmit signals. The channel parameters of top-5 paths are estimated and the variances of those are calculated in Figure 22. The LoS path and the strongest path hold more stable parameters in AoAs, AoDs, and ToFs. We also plot the channel parameter of the LoS and the strongest NLoS path, including their AoA, AoD and relative ToF between the two paths in Figure 23 to 25. The results demonstrate that the AoA and AoD estimations are stable apart from contaminated packets (less than 5 packets out of 100). The relative ToF estimation results fluctuate between 3 and 6 nanoseconds for most of the packets, which leads to some minor localization errors. Moreover, the abnormal relative ToFs, AoAs, and AoDs likely occur in the same packet.

Those abnormal packets are easy to remove in our system by comparing with several neighboring packets.

5.3.10 The Spatial Distribution of Localization Results

The localization dots in a typical indoor environment are shown as scattering points in Figure 26. Each colorful dot represents a location estimate using a single packet, and the black dot indicates the ground truth location. In Figure 26, the dotted line is employed to represent the line-of-sight AoA of the device to be pinpointed. One can observe that most of the dots are spatially distributed along this dotted line, yet their distances to the origin (0, 0) vary. We can conclude that the estimation of AoA is sufficiently accurate over time while the errors in AoDs and ToFs cause a balanced scattering of the estimations on both side of the ground truth along the AoA direction.

5.3.11 Impact of Different Initialization Approaches

To demonstrate the effectiveness of subspace based initialization, we conduct the channel parameter estimation and the device localization under different initialization approaches: i) subspace based initialization (introduced in Section 3.2.2), ii) random initialization, and iii) fixed value initialization (with AoA and AoD being $0°$ and ToF being 10 ns). The resulting localization errors are shown in Figure 27. We can observe that the subspace based initialization outperforms the random and the fixed value initializations. The reason lies in that an improper initialization might lead to local minima, regardless of how many rounds of iterations are executed. The local minima channel parameters will further cause the localization results deviate far away from the real target location.

5.3.12 Time Consumption Analysis

The details of execution time in each step are shown in TABLE 1. The time costs of channel hopping and packet
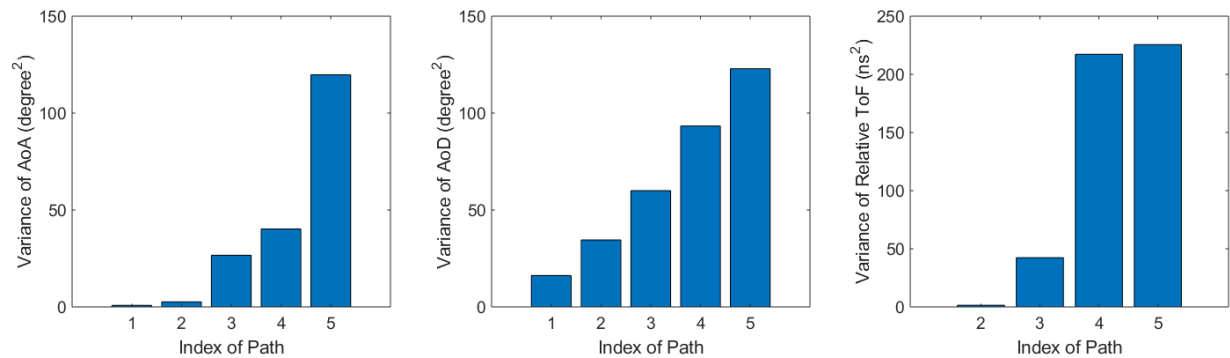
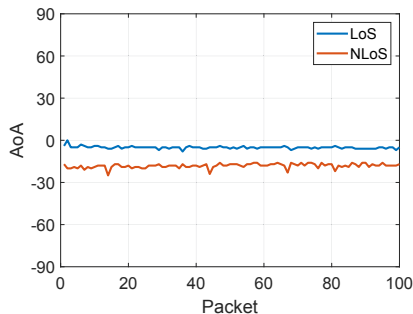Fig. 22: The variances of AoA, AoD and relative ToF of top-5 paths.

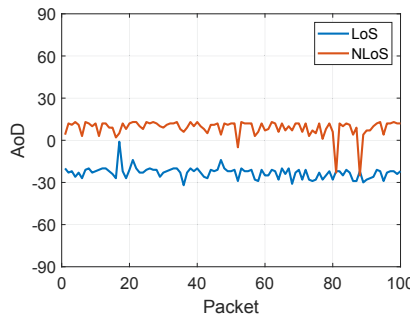Fig. 23: AoA estimation of LoS and NLoS paths.

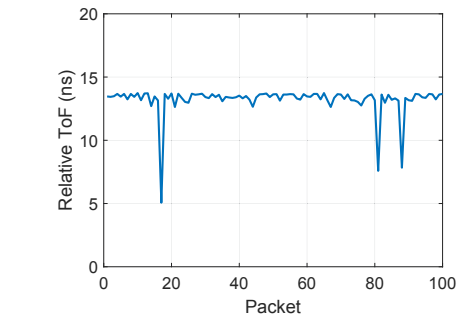Fig. 24: AoD estimation of LoS and NLoS paths.

Fig. 25: Relative ToF estimation between LoS and NLoS paths.
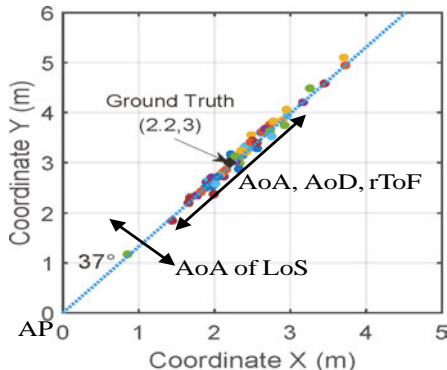

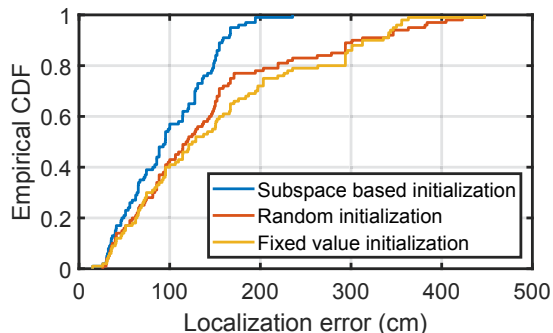Fig. 26: The spatial distribution of localization results

Fig. 27: Localization errors with different initialization approaches.

reception modules in M^3 are negligible. The average switch time of pe42442 chip is only $0.33\mu s$. In each channel, it takes only 1ms to catch a packet and extract effective CSI if the transmitter is configured to send 1000 packets in each second. Therefore, the total time consumption for channel hopping and packet reception is 1ms, 5ms, and 10ms if 1 channel, 5 channels and 10 channels are utilized respec-

tively. The SAGE+ channel parameter estimation procedure, currently executed on a computer using MATLAB software, costs 0.24s, 1.03s and 2.09s on average when CSI from 1 channel, 5 channels, and 10 channels are fed respectively. The time consumption of SAGE+ would be much smaller if it is implemented in binary code. For example, the authors in [44] demonstrate the original SAGE algorithm (one Wi-Fi channel) can achieve less than 0.1s in commercial AP.

6 RELATED WORK

Fingerprint based localization. RADAR [20] is a fingerprint mapping system based on Receive Signal Strength (RSS). The target is localized by mapping the RSS readings from multiple APs with the RSS fingerprint database collected beforehand. Horus [35] improves RSS-based fingerprinting with probabilistic methods, achieving an average of 0.6 meters accuracy. Nonetheless, fingerprint based methods require a RSS database, while collecting fingerprints at many locations entails a large overhead. The work [37] proposed a method to train fingerprints for overhead reduction and quick mapping. The data collection overhead is further reduced via crowd-sourced measurements [37]. Mathematical models are also employed to reduce the overhead [52] [53] [34], but the model-based methods are vulnerable to rich multipaths, thus the localization accuracy is downgraded.

AoA based localization. The work [12] firstly presented ArrayTrack, an AoA based Wi-Fi localization system. For

# Channels	Channel Hopping	Packet Reception	SAGE+
1	$0\mu s$	1ms	0.24s
5	$1.65\mu s$	5ms	1.03s
10	$3.30\mu s$	10ms	2.09s

TABLE 1: Time consumption analysis

a certain AP equipped with multiple antennas, the AoA spectrum is estimated through MUSIC algorithm [38]. The target is localized by combining the spectra of multiple APs. SpotFi [15] designed a novel MUSIC algorithm to obtain AoA and ToF information from OFDM subcarriers simultaneously. AoAs and ToFs from multiple three-antenna APs are synthesized to determine the coordinate of target device. MaTrack [19] proposed a novel *Dynamic-MUSIC* method to extract reflection path for accurate AoA estimation in device-free localization. PinPoint [28] integrated AoA estimation with cyclo-stationary analysis. Phaser [29] contributed on enabling real-time AoA estimation on commercial off-the-shelf (COTS) wireless devices. Side channel information including acceleration and angular momentum is also applied for accurate localization. Ubicarse [27] enables devices to emulate a synthetic aperture radar (SAR). CPUID [16] distinguishes Line-of-Sight (LoS) and non-LoS with data traces from inertial sensors. The authors in [46] make use of the sampling of temporal or spatial wide sense stationary (WSS) signals and utilize a co-prime pair od sparse samples for beamforming and AoA estimation.

However, the aforementioned AoA based localization systems all rely on multiple APs, which is impractical in household and office environments. Besides, the sensor-aided schemes are not ubiquitously applicable because they are hardware-dependent.

Time based localization. Time-based localization with a single AP is quite challenging. Chronos [14] acquired accurate ToF estimations through hopping to plenty of Wi-Fi channels on both 2.4GHz and 5GHz bands. The channel hopping is time-consuming and blocks regular data communication. Sensors of target are also combined with ToF measurements for localization [30]. The authors in [59] proposed a novel ToF estimation scheme and achieved sub-meter localization accuracy on a single three-antenna AP without channel hopping. Time difference of arrival (TDoA) of distributed anchors can also assist Wi-Fi localization. ToneTrack [13] combines CSIs of continuous channels for higher TDoA resolution. Other work [39] [40] [41] can achieve sub-meter level location accuracy at the cost of deployment and synchronization of multiple anchors.

Time based localization schemes do not need APs equipped with a large antenna array, but a large bandwidth is required to refine ToF or TDoA measurements.

Multipath assisted localization and Tracking. Multhpath signal propagation is usually the "enemy" of Wi-Fi indoor localization, hence most of existing systems try to mitigate the reflecting paths. Nevertheless, iLocScan [56] pioneered in exploiting multipath assisted AoA, but the system is built upon USRP and requires eight antennas. The authors in [69] also discussed the powerful multipath assisted localization technology, and its applications in 5G systems. The work [70] proposed a unified theoretical framework to quantify multipath-assisted localization, using the concept of equivalent Fisher information. Lately, *MonoLoco* [63] presented a multipath assisted localization system that extracts AoA, AoD and ToF information of both LoS and NLoS paths using MUSIC algorithm. Authors in [62] formulated a model for joint estimation of AoA, ToF and Doppler shift. The multipath channel information is leveraged to track the

locations (movement) of a device.

Non-Wi-Fi based localization. We also brief on non-Wi-Fi based localization technologies hereby. RFID based technologies including [18] [42] [47] [48] [49] can achieve a high accuracy, but the tag readers are expensive. Acoustic signal processing technologies can also be applied for wireless localization, including audible sound [45] and ultrasonic sound [5] [7]. AALTS [6] utilizes distributed acoustic anchor nodes to locate passive mobile devices. Visible light based localization systems [10] [9] [50] are also proposed. The above works all require additional hardware deployment, hence none of them is ever likely to totally replace the ubiquitous Wi-Fi AP enabled localization.

60GHz based localization. Millimeter Wave (mmWave) such as 60GHz is also a promising solution for indoor localization. The authors in [71] proposed the system based on COTS 60GHz devices that only use coarse CSIs to achieves a sub-meter accuracy. The authors in [72] extended their localization system using the COTS 60GHz devices from 2D to 3D plane, and the results demonstrated a good accuracy too. However, the 60GHz signals are easy to be blocked due to their very short wavelength. Therefore, their applicability may be limited.

7 CONCLUSION

In this paper, we have designed and implemented M^3, a Wi-Fi localization system capable of achieving decimetre-level accuracy with just a single commodity Wi-Fi access point. We have presented a super-resolution algorithm SAGE+ to jointly estimate channel parameters including AoA, AoD, and relative ToF. We have also proposed a novel scheme to combine non-adjacent channels, so as to create a large virtual channel for achieving a higher ToF resolution and accordingly a higher localization accuracy. With the AoA, AoD, and ToF information obtained for each signal path, we have leveraged multipath, albeit traditionally considered "detrimental", to help localize the target device. Extensively experimental results have demonstrated the high localization accuracy of our system in different environments, outperforming the state-of-the-art systems. We believe that the proposed non-adjacent channel combination scheme can benefit a large range of localization and sensing applications requiring a higher time domain resolution. We also present some extended applications of M^3 in Appendix B.

REFERENCES

[1] https://www.infsoft.com/blog-en/articleid/32/indoor-navigation-and-location-based-services-for-shopping-centers, 2015.

[2] U. Rehman and S. Cao, "Augmented-Reality-Based Indoor Navigation: A Comparative Analysis of Handheld Devices Versus Google Glass," In IEEE Trans. on Human-Machine Systems, 2017.

[3] J. Wang, F. Adib, R. Knepper, D. Katabi, and D. Rus, "RF-compass: robot object manipulation using RFIDs," In Proc. of MobiCom 2013.

[4] F. Viani, G. Oliveri, M. Donelli, L. Lizzi, P. Rocca and A. Massa, "WSN-based solutions for security and surveillance," In Proc. of IEEE European Wireless Technology Conference 2010.

[5] N. Priyantha, A. Chakraborty, and H. Balakrishnan, "The Cricket location-support system", In Proc. of the ACM MobiCom 2000.

[6] C. Cai, R. Zheng, J. Li, L. Zhu, H. Pu, and M. Hu, "Asynchronous Acoustic Localization and Tracking for Mobile Targets," in IEEE Internet of Things Journal, 2019.

[7] A. Ward, A. Jones, and A. Hopper, "A new location technique for the active office", IEEE Personal Communications, 1997.

[8] Y. Yelkovan et al., "Infrared beacon based sub-meter indoor localization," In Proc. of IEEE SPCAC 2014.

[9] C. Zhang, and X. Zhang, "LiTell: Robust Indoor Localization Using Unmodified Light Fixtures", In Prof. of ACM MobiCom 2016.

[10] Z. Wang, Z. Yang, J. Zhang, C. Huang, Q. Zhang, "Wearables Can Afford: Light-weight Indoor Positioning with Visible Light", In Proc. of ACM MobiSys 2015.

[11] J. Xiong and K. Jamieson, "Towards fine-grained radio-based indoor location", In Proc. of ACM HotMobile 2012.

[12] J. Xiong, and K. Jamieson, "ArrayTrack: a fine-grained indoor location system," In Proc. of USENIX NSDI 2013.

[13] J. Xiong, K. Sundaresan, and K. Jamieson, "ToneTrack: Leveraging Frequency-Agile Radios for Time-Based Indoor Wireless Localization", In Proc. of ACM MobiCom 2015.

[14] D. Vasisht, S. Kumar and D. Katabi, "Decimeter-Level Localization with a Single WiFi Access Point", In Proc. of USENIX NSDI 2016.

[15] M. Kotaru, K. Joshi, D. Bharadia, and S. Katti, "SpotFi: Decimeter Level Localization Using WiFi", In Proc. of ACM SIGCOMM 2015.

[16] S. Sen, J. Lee, K.-H. Kim, and P. Congdon, "voiding multipath to revive inbuilding wifi localization", In Proc. of ACM MobiSys 2013.

[17] Z. Chen, Z. Li, X. Zhang, G. Zhu, Y. Xu, J. Xiong, and X. Wang. "AWL: Turning Spatial Aliasing From Foe to Friend for Accurate WiFi Localization", In Proc. of ACM CoNEXT 2017.

[18] J. Wang, D. Vasisht, and D. Katabi, "RF-IDraw: virtual touch screen in the air using RF signals", In Proc. of ACM SIGCOMM 2014.

[19] X. Li, S. Li, D. Zhang, J. Xiong, Y. Wang and H. Mei, "Dynamic-MUSIC: Accurate Device-Free Indoor Localization", in Proc. of ACM UbiComp 2016.

[20] P. Bahl and V. Padmanabhan, "RADAR: An in-building RF-based User Location and Tracking System", In Prof. IEEE INFOCOM, 2000.

[21] http://www.samsung.com/global/galaxy/galaxy-s9/specs/, 2019.

[22] Matthew Gast. "802.11ac: A Survival Guide (1st ed.)", O'Reilly Media, Inc. 2013.

[23] Z. Chen, X. Zhang, S. Wang, Y. Xu, J. Xiong and X. Wang, "BUSH: Empowering large-scale MU-MIMO in WLANs with hybrid beamforming," IEEE Proc. of INFOCOM 2017.

[24] A. Lemma, A. Veen and Ed F. Deprettere, "Analysis of joint angle-frequency estimation using ESPRIT," In IEEE Trans. Signal Proc 2003.

[25] J. Xiong, K. Jamieson, and K. Sundaresan,"Synchronicity: pushing the envelope of fine-grained localization with distributed mimo", In Proc. of ACM HotWireless 2014.

[26] D. Halperin, W. Hu, A. Sheth, and D. Wetherall, "Tool release: gathering 802.11n traces with channel state information", ACM SIGCOMM Comput. Commun. Rev.

[27] S. Kumar, S. Gil, D. Katabi, and D. Rus, "Accurate indoor localization with zero start-up cost," In Proc. of ACM MobiCom 2014.

[28] K. Joshi, S. Hong, and S. Katti, "PinPoint: Localizing Interfering Radios", In Proc. of USENIX NSDI 2013.

[29] J. Gjengset, J. Xiong, G. McPhilips, and K. Jamieson, "Phaser: Enabling phased array signal processing on commodity Wi-Fi access points", In Proc. of ACM MobiCom 2014.

[30] A. T. Mariakakis, S. Sen, J. Lee, and K.-H. Kim, "Sail: Single access point-based indoor localization", In Proc. of ACM MobiCom 2014.

[31] S. Lanzisera, D. Zats, and K. Pister, "Radio Frequency Time-of-Flight Distance Measurement for Low-Cost Wireless Sensor Localization", IEEE Journal on Sensors, 2011.

[32] D. Tse and P. Viswanath, "Fundamentals of Wireless Communication", Cambridge University Press, 2005.

[33] Y. Xie, Z. Li, and M. Li, "Precise Power Delay Profiling with Commodity WiFi", In ACM Proc. of MobiCom 2015.

[34] H. Lim, C. Kung, J. Hou, and H. Luo, "Zero configuration robust indoor localization: Theory and experimentation", In Proc. of IEEE Infocom 2006.

[35] M. Youssef and A. Agrawala, "The Horus WLAN location determination system", In Proc. of ACM MobiSys 2005.

[36] E. Schubert, J. Sander, M. Ester, H. P. Kriegel, and X. Xu, "DB-SCAN Revisited, Revisited: Why and How You Should (Still) Use DBSCAN". ACM Trans. Database Syst, 2017.

[37] A. Haeberlen, E. Flannery, A. Ladd, A. Rudys, D. Wallach, and L. Kavraki, "Practical robust localization over large-scale 802.11 wireless networks", In Proc. of ACM MobiCom 2004.

[38] R. Schmidt, "Multiple emitter location and signal parameter estimation", IEEE Trans. on Antennas and Propagation, 1986.

[39] S. Lanzisera, D. Zats, and K. Pister, "Radio Frequency Time-of-Flight Distance Measurement for Low-Cost Wireless Sensor Localization", IEEE Journal on Sensors, 2011.

[40] S. A. Golden and S. S. Bateman, "Sensor measurements for wi-fi location with emphasis on time-of-arrival ranging", IEEE Trans. on Mobile Computing, 2007.

[41] F. Zhao, W. Yao, C. C. Logothetis, and Y. Song, "Super-resolution toa estimation in ofdm systems for indoor environments", In Proc. IEEE ICNSC 2007.

[42] J. Wang and D. Katabi, "Dude, where's my card?: Rfid positioning that works with multipath and non-line of sight", In Proc. ACM SIGCOMM 2013.

[43] B. H. Fleury, M. Tschudin, R. Heddergott, D. Dahlhaus, and K. Ingeman Pedersen, "Channel parameter estimation in mobile radio environments using the SAGE algorithm, In IEEE J. Select. Areas Commun, 1999.

[44] Y. Xie, J. Xiong, M. Li, and K. Jamieson, "mD-Track: Leveraging Multi-Dimensionality for Passive Indoor Wi-Fi Tracking," in Proc. of the ACM MobiCom, 2019.

[45] N. Xiang , D. Bush , and J. Summers , "Experimental validation of a coprime linear microphone array for high-resolution direction-of-arrival measurements", J. Acoust. Soc. Am., 2015.

[46] P. P. Vaidyanathan and P. Pal, "Sparse Sensing With Co-Prime Samplers and Arrays", In IEEE Trans. on Signal Processing, 2011.

[47] J. Wang, F. Adib, R. Knepper, D. Katabi, and D. Rus, "Rf-compass: robot object manipulation using rfids", In Proc. of ACM MobiCom 2013.

[48] L. Yang, Y. Chen, X. Li, C. Xiao, M. Li, and Y. Liu. "Tagoram: real-time tracking of mobile RFID tags to high precision using COTS devices", In Proc. of ACM MobiCom 2014.

[49] L. Yang, Y. Li, Q. Lin, X. Li, and Y. Liu, "Making sense of mechanical vibration period with sub-millisecond accuracy using backscatter signals", In Proc. of MobiCom 2016.

[50] S. Zhu, and X. Zhang, "Enabling High-Precision Visible Light Localization in Today's Buildings", In Proc. of ACM MobiSys 2017.

[51] A. Rai, K. K. Chintalapudi, V. N. Padmanabhan, and R. Sen, "Zee: Zero-effort Crowdsourcing for Indoor Localization", In Proc. of ACM MobiCom 2012.

[52] K. Chintalapudi, A. Padmanabha Iyer, and V. N. Padmanabhan, "Indoor Localization without the Pain", In Proc. of ACM MobiCom, 2010.

[53] Y. Gwon and R. Jain, "Error characteristics and calibration-free techniques for wireless LAN-based location estimation", In Proc. ACM MobiWac 2004.

[54] M. Wax and T. Kailath, "Detection of signals by information theoretic criteria," in IEEE Trans. Acoustics, Speech, and Signal Processing 1985.

[55] T. K. Moon, "The expectation-maximization algorithm," in IEEE Signal Processing Magazine, vol. 13, no. 6, pp. 47-60, Nov 1996.

[56] C. Zhang, F. Li, J. Luo, and Y. He, "iLocScan: harnessing multipath for simultaneous indoor source localization and space scanning", In Proc. of ACM SenSys 2014.

[57] G. J. McLachlan, T. Krishnan, "The EM Algorithm and Extensions (Wiley Series in Probability and Statistics)", 2008

[58] D. Halperin, W. Hu, A. Sheth, and D. Wetherall, "Tool release: gathering 802.11n traces with channel state information", SIGCOMM Comput. Commun. Rev. 2011.

[59] W. Gong and J. Liu, "SiFi: Pushing the Limit of Time-Based WiFi Localization Using a Single Commodity Access Point", in Proc. ACM Interact. Mob. Wearable Ubiquitous Technol., 2018.

[60] X. Li, L. D. Zhang, Qin, J. Xiong, S. Li, Y. Zhang and H. Mei, "IndoTrack: Device-Free Indoor Human Tracking with Commodity Wi-Fi", in Proc. of ACM IMWUT 2017.

[61] K. Qian, C. Wu, Z. Yang, Y. Liu and K. Jamieson, "Widar: decimeter-level passive tracking via velocity monitoring with commodity wi-fi", in Proc. of ACM MobiHoc 2017.

[62] K. Qian, C. Wu, Y. Zhang, G. Zhang, Z. Yang and Y. Liu, "Widar2.0: Passive human tracking with a single wi-fi link", in Proc. of ACM Mobisys 2018.

[63] E. Soltanaghaei, A. Kalyanaraman and K. Whitehouse, "Multipath Triangulation:Decimeter-level WiFi Localization and Orientation with a Single Unaided Receiver", in Proc. of ACM MobiSys 2018.

[64] T. Wei, A. Zhou and X. Zhang, "Facilitating Robust 60 GHz Network Deployment By Sensing Ambient Reflectors", In Proc. of USENIX NSDI 2017.

[65] WARP Project, http://warpproject.org, 2019.

[66] J. Lin, W. Fang, Y. Wang and J. Chen, "FSF MUSIC for Joint DOA and Frequency Estimation and Its Performance Analysis," in IEEE Trans. on Signal Processing, 2006.

[67] Yung-Yi Wang, Jiunn-Tsair Chen and Wen-Hsien Fang, "TST-MUSIC for joint DOA-delay estimation," in IEEE Trans. on Signal Processing, 2001.

[68] Orfanidis, S J. "Electromagnetic Waves and Antennas.", Macmillan Publishing Co., New York, 2010.

[69] K. Witrisal et al., "High-Accuracy Localization for Assisted Living: 5G systems will turn multipath channels from foe to friend," in IEEE Mag. on Signal Processing, 2016.

[70] E. Leitinger, P. Meissner, C. Rüdisser, G. Dumphart and K. Witrisal, "Evaluation of Position-Related Information in Multipath Components for Indoor Positioning," in IEEE J. on Selected Areas in Communications, 2015.

[71] G. Bielsa, J. Palacios, A. Loch, D. Steinmetzer, P. Casari and J. Widmer, "Indoor Localization Using Commercial Off-The-Shelf 60 GHz Access Points," in Proc. of the IEEE INFOCOM, 2018.

[72] I. Pefkianakis and K. Kim, "Accurate 3D Localization for 60 GHz Networks," in Proc. of the ACM SenSys, 2018.

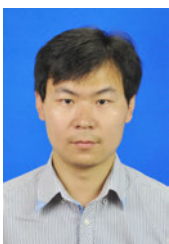[73] M. Kotaru, S. Katti, "Position Tracking for Virtual Reality Using Commodity Wi-Fi," In Proc.of IEEE CVPR, 2017.

Jie Xiong received the B.Eng. degree from Nanyang Technological University, Singapore, in 2005, the M.Sc. degree from Duke University, Durham, NC, USA, in 2009, and the Ph.D. degree in computer science from University College London, London, U.K., in 2015. He is an Assistant Professor in the College of Information and Computer Sciences UMass Amherst, USA. His research interests include building practical wireless and mobile systems that bridge the gaps between theory and reality. His recent work appears at MobiCom, NSDI, CoNEXT, Ubicomp, and INFOCOM. Prof. Xiong was the recipient of the prestigious Google European Doctoral Fellowship in Wireless Networking for his doctoral studies. His Ph.D. thesis was the 2016 British Computer Society Distinguished Dissertation Award runner-up.

Zhe Chen is a research fellow in Nanyang Technological University, Singapore. He received the Ph.D. degree with honor in Computer Science from Fudan University, Shanghai, China in 2018. He received the Doctoral Dissertation Award from ACM SIGCOMM China 2019. His research interests include designing and implementing system for practical large-scale MU-MIMO systems, deep learning and Internet-of-Things application.

Jin Zhao received the B.Eng. degree in computer communications from Nanjing University of Posts and Telecommunications, China, in 2001, and the Ph.D. degree in computer science from Nanjing University, China, in 2006. He joined Fudan University as an assistant professor in 2006. His research interests include P2P networks, media streaming and network coding theory. He is a member of IEEE and ACM.

Guorong Zhu received the M.S. degree in Computer Science with honor from Fudan University in 2019. His research interests include wireless networking, wireless security and mobile computing.

Jun Luo received his BS and MS degrees in Electrical Engineering from Tsinghua University, China, and the Ph.D. degree in Computer Science from EPFL, Lausanne, Switzerland. From 2006 to 2008, he has worked as a postdoctoral research fellow in the Department of Electrical and Computer Engineering, University of Waterloo, Waterloo, Canada. In 2008, he joined the faculty of the School Of Computer Science and Engineering, Nanyang Technological University in Singapore, where he is currently an Associate Professor. His research interests include mobile and pervasive computing, wireless networking, applied operations research, as well as network security.

Sulei Wang received the M.S. degree in Electronic Engineering with honor from Fudan University in 2019 and the B.Eng. degree in Electronic Engineering from Shandong University in 2016. His research interests include wireless networking, wireless security and mobile computing.

Xin Wang received the B.S. degree and the M.S. degree from Xidian University, Xi'an, China, in 1994 and 1997 respectively, in Information Theory and Communications. He received the Ph.D. degree from Shizuoka University, Japan in 2002, in Computer Science. Since 2002, he has been with the School of Computer Science at Fudan University, where he is currently a full professor. In 1995 and 1998, he was working on China's pioneering telecom-level video conferencing systems and DVB-S systems with Huawei Inc.

Yuedong Xu received B.S. degree from Anhui University in 2001, M.S. degree from Huazhong University of Science and Technology in 2004, and Ph.D. degree from The Chinese University of Hong Kong, Hong Kong, China, in 2009. He is a tenured Associate Professor with the School of Information Science and Technology, Fudan University, Shanghai, China. From late 2009 to 2012, he was a Postdoc with INRIA Sophia Antipolis and Universite d'Avignon, France. His research interests include performance evaluation, security, data analytics and economic analysis of communication networks and mobile computing.

APPENDIX A
CALIBRATION SCHEMES FOR AOA AND AOD

The basic calibration scheme, also called local calibration, is inspired by some recent work [12], [29], [73]. The transmitter and the receiver are put together and are connected via RF cables to measure the phase offsets of RF chains, as shown in Figure 28. We start from a simple scenario with two transmit antennas and two receive antennas for ease of interpretation. The phases of received signal at the receiver is given by

$$d = \left\{ \begin{array}{cc} a_1 + b_{11} + c_1 & a_2 + b_{12} + c_1 \\ a_1 + b_{21} + c_2 & a_2 + b_{22} + c_2 \end{array}, \right\} \tag{12}$$

where a_i denotes the phase of the ith transmit antenna, c_i is that of the ith receive antenna, and b_{ij} is the phase rotation between the ith transmit and the jth receive antennas in cables, for $i, j \in \{1, 2\}$, respectively. Due to spatial multiplexing issues, same length for each coaxial cable will make Wi-Fi cards failed to decode packets. Therefore, the channel phase matrix $\mathbf{b} = \begin{bmatrix} b_{11} & b_{12} \\ b_{21} & b_{22} \end{bmatrix}$ is tuned by configuring the different lengths of coaxial cables. The channel phase matrix is known beforehand and the purpose of phase calibration is to resolve the unknown phases of the transmit and receive antennas. After removing the known $\mathbf{b}$ from $\mathbf{d}$ and cancelling out the first element subsequently, we obtain an alternative matrix of phase offsets by

$$d_c = \left\{ \begin{array}{cc} 0 & a_2 - a_1 \\ c_2 - c_1 & a_2 - a_1 + c_2 - c_1 \end{array} \right\}. \tag{13}$$
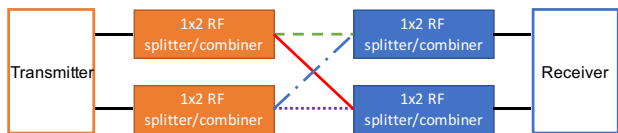

Fig. 28: The local (traditional) calibration scheme

As a practical limitation of local calibration, both the transmitter and the receiver should be placed together when either of them is powered on or reset. Therefore, we present a separated calibration scheme to reduce the burden of calibration. We use a pair of Wi-Fi cards, instead of one, at the transmitter and the receiver as shown in Figure 29. One Wi-Fi card is the main card for positioning and communication, the other is auxiliary and used for calibration so that the calibrations of AoA and AoD are executed separately. The matrix of phase offsets at the transmitter is expressed as

$$d_c^t = \left\{ \begin{array}{cc} 0 & a_2 - a_1 \\ c_2^c - c_1^c & a_2 - a_1 + c_2^c - c_1^c \end{array} \right\}, \tag{14}$$

where c_i^c is the phase of the ith receive antenna of the auxiliary Wi-Fi card for $i \in 1, 2$. Similarly, the matrix of phase offsets of the receiver is expressed as

$$d_c^r = \left\{ \begin{array}{cc} 0 & a_2^c - a_1^c \\ c_2 - c_1 & a_2^c - a_1^c + c_2 - c_1 \end{array} \right\} \tag{15}$$

where a_i^c is the phase of the ith transmit antenna of the auxiliary Wi-Fi card. Given d_c^t and d_c^r, the second and the third elements of d_c are obtained directly, and the last element is obtained by subtracting the first column of d_c^r
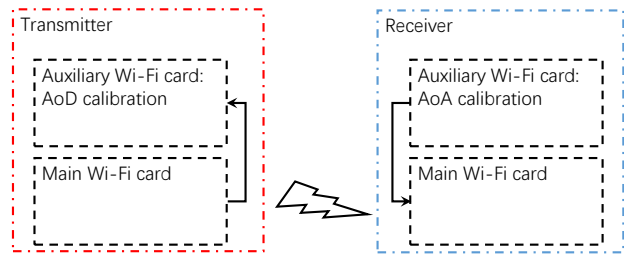

Fig. 29: The separated calibration scheme

from the first row of d_c^t. This linear operating approach can be easily generalized to any $N \times N$ MIMO system. The main advantage of separated calibration is relieving the burden of local calibration that may need to move transmitter and the receiver in each RF reset. Although the phase calibration introduces extra operations, it can be solved simply using an inexpensive RF switch such as F2933 chipset (designed by Integrated Device Technology, Inc.).

APPENDIX B
EXTENDED APPLICATIONS

B.1 Mutual Localization

We hereby propose to generalize M^3 to mutual localization, a new application enabling multiple devices to pinpoint each other's relative positions without the support of infrastructure. The mutual localization has a great potential in robots positioning where the neighbouring devices need to gauge their relative distances. We conduct the first mutual localization study using Wi-Fi.

Our system M^3 can be directly applied to mutual localization by swapping the transmitter and the receiver. We consider a more promising scenario where two neighbouring devices can communicate with each other for collaborative localization. According to Subsection 5.2.1 and 5.2.2, the estimated AoA is intrinsically more accurate than the estimated AoD. Therefore, if the estimated AoD of a link is substituted by the estimated AoA of its reverse link, a more accurate positioning is likely to be reached. We test 25 locations in the meeting room (Figure 9) and plot the CDF of localization accuracy in Figure 30. Here, AoA_AoD indicates the original approach in M^3 and AoA_AoA indicates the approach of AoD replacement. We observe that the latter improves the median error of localization by 15 cm compared with the former. One take-home message is that the mutual localization can benefit from the cooperation of both devices.
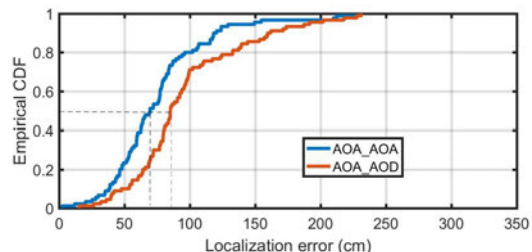

Fig. 30: Performance of mutual localization with and without AoD replacement

A common mutual localization scenario usually involves more than a single pair of devices. Here, we consider a more complicated square "topology" with four devices labeled as **A**, **B**, **C** and **D** In Figure 31. Each edge is 4 meters long in the meeting room. When one of the devices transmits signal, all the other three estimate its relative locations. These devices act as the transmitter sequentially and the AoD replacement is adopted to improve the accuracy of localization. Figure 31 illustrates the estimated positions of **A** where different marks refer to the positioning at different receiving devices. For each set of estimated locations by a receiver, we simply use K-means approach to cluster them into two groups. The clustering center that covers a majority of locations is deemed as the estimated location of the device. We then take the average of three positions of **A** estimated by **B**, **C** and **D** to finally pinpoint the location of **A**. Figure 31 shows the estimated topology through mutual localization. The estimated topology almost retains the original square shape and only gently deviates from their ground truth locations.
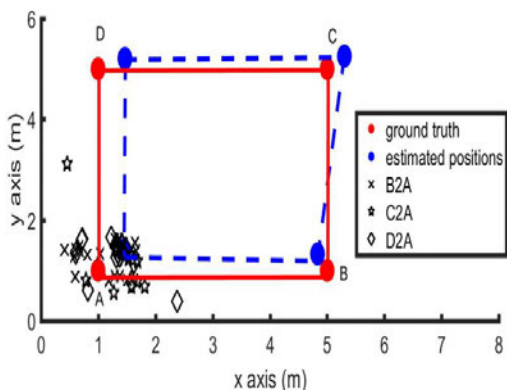

Fig. 31: The estimated topology through mutual localization.

B.2 Wi-Fi Geo-Fencing

The competent performance of M^3 may also enable us to create a virtual (indoor) Geo-Fencing for various public areas where free Wi-Fi is available. M^3 can measure the location of every person's distribution in the room and count the most popular area of this place. We divide a classroom into four areas and conduct 50 experiments to illustrate the capability. And in these experiments, we place the antennas at a randomly chosen location in the classroom (Figure 9). According to the results, We find that M^3 can achieve an average of 88% detection accuracy. According to our investigation, most of errors appear if the transmitters are placed near to the boundaries of the areas.

APPENDIX C
DISCUSSIONS

While M^3 can achieve a nice performance, some limitations still exist and need to be discussed.

Localizing in NLoS condition. One limitation of M^3 is that it relies on the direct path between transmitter and receiver. According to Section 5, the evaluation shows that M^3 can perform well even in NLoS scenarios (blocked by wood bricks) where the direct path is attenuated by the

obstacles. However, if the direct path disappears, M^3 will fail to locate the target device. Actually, dealing with the no direct path scenario is a common challenge for all Wi-Fi based localization systems, and how to overcome this limitation is still an open problem [12], [17], [63].

Coordinating multiple APs is able to solve the above problem. The device to be located can be heard by all APs even it does not connect to all of them. Then, we can choose one of the strongest signal among all APs or combine multiple signals from APs to perform localization.

Localizing in First Order Reflection Blockage. We leverage the first order reflection to assist localization in our system. Generally, there may exist more than one first-order reflections in a room. If one of them is blocked, we may still have the chance to identify the other first-order reflection paths. Moreover, the user can move slightly to "create" more first order reflections with little effort.

Localizing in 3D space. Our current work only considers localization in a 2D space instead of a 3D space. We present the reason below and discuss how to achieve localization in 3D. Mobile devices including smartphones, laptops, and tablet computers are equipped with a few antennas (e.g. three antennas) because of the limited size of devices. As a result, the 3-element linear antenna array can only estimate the horizontal azimuth plane, but not the vertical azimuth plane [68]. To achieve 3D localization, more antennas are needed. To build a 3D localization system, we can use a 2D antenna array such as a circular array, or rotate a linear antenna array manually. Owing to the limitation of commodity Wi-Fi cards (i.e., few antennas and linear antenna array), we do not consider 3D localization in this work. Our future study will employ a software defined radio (SDR) platform to assess the accuracy of 3D localization that can be equipped with more antennas and hence support more complicated antenna arrays.